Mechanical Imaging of Soft Tissues with a Highly Compliant Tactile Sensing Array

Bin Li, *Student Member, IEEE,* Ye Shi, *Student Member, IEEE,* Adam Fontecchio, *Senior Member, IEEE* and Yon Visell, *Member, IEEE*

***Abstract*—Objective: The mechanical imaging of lumps in tissues via surface measurements can permit the noninvasive detection of disease-related differences in body tissues. We present and evaluate sensing techniques for the mechanical imaging of soft tissues, using a highly compliant electronic sensing array. Methods: We developed a mechanical imaging system for capturing tissue properties during automatic or human-guided palpation. It combines extremely compliant capacitive tactile sensors based on soft polymers and microfluidic electrodes with custom electronic data acquisition hardware, and new algorithms for enhanced tactile imaging by reference to nominal tissue responses. Results: We demonstrate that the system is able to image simulated tumors (lumps), yielding accurate estimates of cross section area independent of embedding depth. In addition, as a proof of concept, we show that similar tactile images can be obtained when the sensor is worn on a palpating finger. Conclusion: Soft capacitive sensors can accurately image lumps in soft tissue provided that care is taken to control and compensate for electrical and mechanical background signals. Significance: The results underline the utility of soft electronic sensors for applications in medical imaging or clinical practices of palpation.**

***Index Terms*—lump detection, tactile sensing, stretchable sensing, imaging, capacitive sensor**

I. Introduction

TACTILE elasticity imaging, or tactile elastography, aims to reconstruct the composition of a volume of tissue from surface mechanical measurements, in the form of stress (normal pressure and shear traction) or strain (displacement) captured by a measurement instrument. It is a valuable alternative to other imaging modalities, because it is relatively non-invasive, and able to capture surface mechanics of tissues that reflect the elasticity of sub-surface tissues. As detailed below, several methods for tactile mechanical imaging are described in the literature, and a few have reached clinical application. However, most approaches utilize sensing devices that are many orders of magnitude stiffer than body tissues. Mechanical imaging techniques based on softer sensors, like that presented here, could facilitate imaging of sensitive, curved, hard, or heterogeneous tissues, and could yield wearable sensors that are able to capture quantitative data during existing clinical physical examination practices (Fig. 1).

Yon Visell is with the Department of Electrical and Computer Engineering, Media Arts and Technology Program, and California NanoSystems Institute, University of Califonia, Santa Barbara, California 93106, USA e-mail: yonvisell@ece.ucsb.edu

Bin Li, Ye Shi and Adam Fontecchio are with the Department of Electrical and Computer Engineering, Drexel University, Philadelphia, PA, 19104 USA. e-mail: bin.li@drexel.edu

In medicine, palpation refers to the application of touch in the physical examination of the body, and represents an essential clinical skill. Physicians palpate with the hand or finger to assess the condition of body organs or tissues, and to aid in disease diagnosis. In many cases, including breast and prostate cancer, palpation remains the first opportunity, lowest cost, and least invasive method for detecting cancer. However, physicians often miss nodules or lumps, due to tissue inhomogeneities, perceptual limitations in what can be felt, or to incorrect technique [1], leading to diagnostic errors. Equally concerning, most physical examinations currently yield little quantitative information. This can make diagnosis and prognosis error prone, and can impede tracking of disease progression over time. Tumors are usually much stiffer than healthy soft tissue [2–4]. This distinction in stiffness makes it possible to use electronic tactile sensors to non-invasively detect and assess subsurface lumps [5–11].

A diverse variety of sensing methods for tactile imaging or elastography have been studied for the detection of tissue lumps or other features. Prevailing technologies have been based on optically-based mechanical sensing [12, 13], capacitive strain sensing [14], and rigid point-force sensors based on resistive, piezoelectric and magnetic principles [8, 11, 15, 16]. Devices involved in tactile imaging frequently employ sensors distributed over rigid substrates, and as a result cannot conform to heterogeneous, stiff, highly curved, or sensitive bodily tissues. In contrast, soft, conformable sensors, like that proposed here, are readily adapted to such application requirements, and can also yield high quality data, as we demonstrate, but have rarely been studied for the tactile imaging of tissues.

Within the broader field of mechanical sensing, several strategies have recently been developed for realizing mechanical sensors from stretchable materials [17–23], or somewhat stiffer polydimethylsiloxane (PDMS) [24, 25], or from flexible substrates [26–29], or through other geometric specializations, such as meshing [30–33]. The method of embedding liquid metal Gallium Indium alloy within soft synthetic polymers was first used to realize simple assemblies of point strain sensors [17, 18]. In our previous work, we combined soft polymer sensors with capacitance sensing methods to realize highly conformable distributed tactile sensing arrays [22, 23, 34]. The intrinsic compliance of the these polymer composite sensors allows them to conform to a wide range of surfaces, while their predictable electronic and mechanical behavior ensure consistent (high) performance, suggesting that they would prove useful for biomedical problems of mechanical imaging. However, none of the aforementioned devices has previously

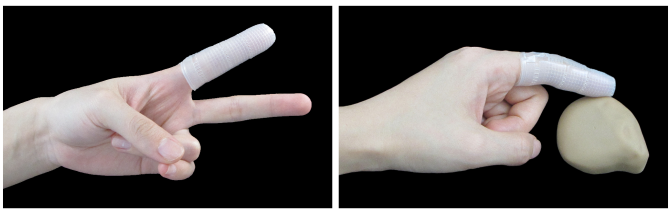

Fig. 1: Wearable sensing prototypes based on a similar device design to that employed in this paper. Such sensors may prove useful for wearable sensing during physical examinations by palpation.

been investigated for this purpose.

Beyond sensor design, a second problem in tactile imaging is to infer the properties of palpated tissue from surface measurements. Using the latter, the goal is often to extract information, in the form of images $I(x, y)$ or volumetric data $E(x, y, z)$, that reflects the spatial distribution of tissue properties (typically elasticity). Although this entails a reconstruction problem that is, in general, ill-posed, several methods have been proposed for imaging and enhancement from tactile sensor measurements, based on the processing of single images [35], relative comparisons of multiple images [16, 36–38], or direct estimation of tissue properties [37, 39]. The utility of computational enhancement methods for tactile images captured with a compliant sensor array has not been previously studied. In the present contribution, we demonstrate new methods for enhancing and extracting invariant features of lumps embedded in tissues from surface measurements captured with a highly compliant sensor.

In order to address these challenges at the device level, we recently developed tactile sensors and sensing techniques that are intrinsically deformable [34]. These sensors use arrays of liquid metal electrodes embedded in multilayer soft polymer membranes (Figure 4). Their low elastic modulus enables them to compliantly conform to touched surfaces that are themselves curved or compliant. Our prior work provides a review of the overarching design principles for these sensors, and a detailed characterization of their geometric, mechanical, and electronic

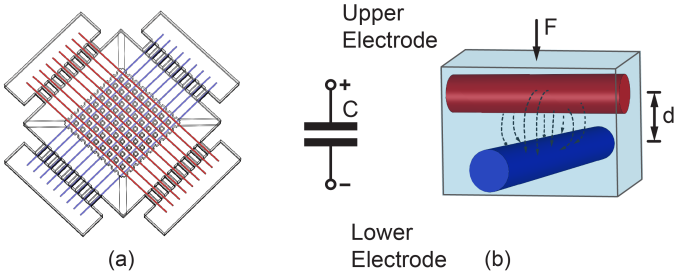

Fig. 2: Illustration of the operating principle, based on capacitive sensing. a) Configuration of the two orthogonally arranged layers of microchannel electrodes, highlighted in red and blue colors, respectively. b) The sensing elements consist of upper and lower electrodes.

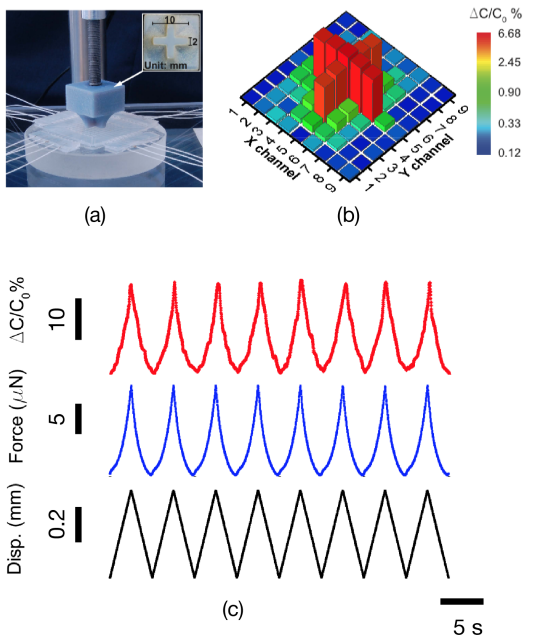

Fig. 3: The sensors were evaluated via indentation testing (a), yielding measurements with excellent performance in response to spatially (b) or repeated temporally (c) varying loads.

properties, and performance characteristics [23, 34].

In the research presented here, we investigated the mechanical imaging of soft tissues using a unique, soft tactile sensing system suitable for imaging tumors or other lesions in body tissues. We realized extremely compliant tactile sensors, based on soft polymers, that were fabricated using soft lithography techniques, and microfluidic electrodes for capacitance sensing. We combined these devices with custom electronics for data acquisition, and numerical algorithms for enhancing lumps in tactile images. To assess this approach to mechanical imaging, we fabricated an array of simulated (polymer) tissues with embedded lumps (simulating tumors). We demonstrate that our system is able to automatically produce images of the subsurface lumps of varying size and depth, and, using multi-image enhancement methods, we show that it is possible to capture the geometry of embedded lumps with results that are nearly independent of embedding depth. As a proof of concept that demonstrates the unique capabilities of our sensing methods, we also show that similar tactile images are obtained when the load is applied by a human finger that palpates the tissue via the sensor, pointing toward the possibility of examination gloves that might perform biomedical sensing during routine physical examinations. The remainder of the paper describes the sensing devices, sensing system, and computational methods, and the simulated tissues used to evaluate it.

II. Measurement Instrument: Soft Tactile Sensor

Tactile signals from palpated subsurface lumps are diminished due to the intervening tissue, and spatial definition in the tactile signals is also lost. To ensure that such lumps could be imaged accurately, we used principles developed in our recent

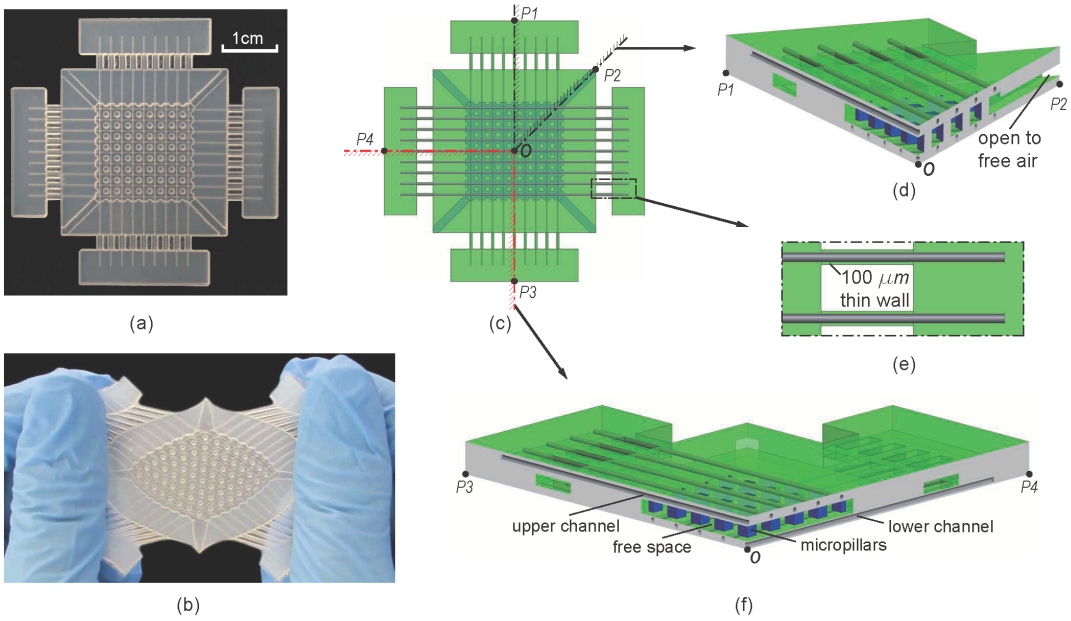

Fig. 4: Overview of the multilayer stretchable tactile sensing arrays. a) The 9 × 9 tested sensor array. b) Demonstration of the softness of the sensing array. c-f) Illustration of the structure of the soft sensing array, showing the configuration of microchannels and micropillars.

work [23, 34] to fabricate tactile sensors with high spatial resolution, sensitivity, and to ensure excellent performance in both static and dynamic sensing conditions.

a) Sensing method: The operating principle of the tactile imaging device is based on changes in the mutual capacitance between arrays of microfluidic electrodes arranged on two orthogonal planes. Changes in capacitance result from geometric deformations of the electrodes under mechanical loading of the membrane (Figure 2). When the (soft) sensor is pressed against an object, local deformation near the closest approach of a pair of microfluidic electrodes yields a change in the distance between them, and an increase in mutual capacitance.

As demonstrated in our previous work, the change in the device geometry accompanying deformation accurately reflects the resulting change in mutual capacitance that is sensed [23]. This capacitance change thus reflects the local strain, and, indirectly, the normal pressure applied to the sensor in this region. In capacitance sensing, the dielectric properties of the environment, and fringing electric fields, can also affect the sensor performance. We minimized these effects through the use of careful electronic design and (dynamic) idle channel grounding (Section IIIA). Differential imaging in software (Section IIIC) also aided in reducing these artifacts.

The resulting sensors prove accurate and responsive (Fig. 3), with high repeatability and low levels of hysteresis during loading and unloading, due to the thin profile of the device. After calibration, we have demonstrated that we can obtain an estimate of local strain or pressure at each point on the sensor surface that is accurate to about 1%, and a nearly linear variation in capacitance is observed as a function of force. Under displacement-controlled loading, capacitance rises monotonically by 25% under an imposed strain that increased by 30%, yielding, at minimum (i.e., within this range), 42 dB of dynamic range. Cross-talk to adjacent (unpressed) sensing cells is minimal, less than 1% [23, 34].

b) Sensor structure: The sensing array consists of a thin, composite membrane, comprised of three layers (Figure 4). Briefly, each layer is fabricated from low modulus addition-cured synthetic polymer, ensuring high levels of compliance. We combine layers to yield thin, multilayer membranes [34]. The electrodes are embedded into top and bottom polymer layers via microfluidic channels that are filled with a metal alloy that is liquid at room temperatures and above (eutectic Gallium Indium, eGaIn, 75% Ga, 25% In by mass, melting point 15.7 °C [40, 41]). Between these layers is a third layer, comprising a two-dimensional array of micropillars, which make it possible to tune the operating range of pressures and the electronic sensitivity of the device to application requirements. Four electronic interface elements are offset from the main membrane, which serve to insulate the microchannel and electrical interconnects from mechanical stress during testing. Due to the low elastic modulus of the soft polymer substrate, the sensing devices can recoverably deform to applied strains greater than 200% without mechanical or electronic damage.

c) Tactile imaging of hard lesions in soft tissue: The sensing area comprises an array of elements near the intersection of each pair of orthogonally arranged electrodes. The sensor is coupled to a data acquisition system that provides a value c_{ij} giving the mutual capacitance between each row electrode i and column electrode j. Using calibration data, this capacitance value c_{ij} can be converted to a force per unit area, i.e. pressure, p_{ij}, associated with each sensing element ij. Because the tissues themselves are soft, stresses change slowly across the surface of the sensor, and it is possible to interpolate pressure values to obtain a continuous measure, $p(x)$ (see Results, below).

In a volume of heterogeneous tissue, the variation in Young's modulus with position yields differences in the ef-

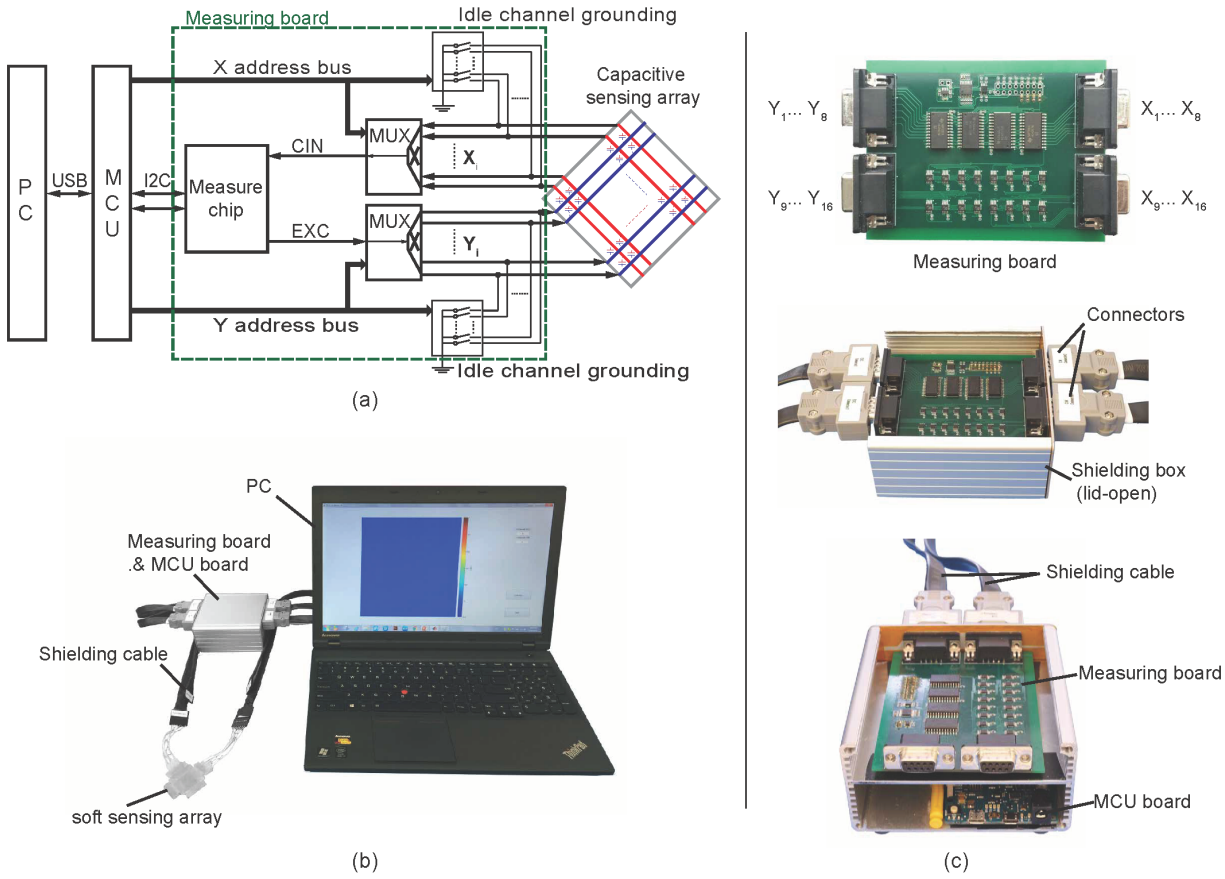

Fig. 5: Tactile sensing system design and implementation. a) The simplified schematic of the sensing system. b) The complete assembly of the tactile sensing system. c) The assembled data acquisition and microcontroller circuits, capable of scanning through up to 16×16 sensing cells.

fective stiffness, or, more generally, the displacement-pressure relation $P(x, y) \equiv P(u(x, y))$ between normal pressure P and displacement $u(x, y)$ at a surface point (x, y). During sensing, these tissue differences will be reflected in variations in the measured pressure $P(x, y)$ at the interface with the sensor. Pressure will be highest at areas directly above a lesion of high Young's modulus compared to the tissue, and, for tissue volumes that are large compared to the lump size, will be higher when the lesion is closer to the surface. In addition, a larger lump will yield a wider distribution of high pressure values. Computing the volumetric variation in Young's modulus due to a lump from surface measurements would require solving an ill-posed inverse problem. However, as we disclose below, with appropriate assumptions on the geometry of the lump, it is possible to use image processing to extract reliable size estimates independent of depth or applied surface load.

III. Experiments

In order to empirically investigate the use of soft tactile sensors for imaging lumps in tissue, we designed and fabricated a tactile sensing system to perform tactile imaging of a variety of simulated tissues, and developed multi-image enhancement algorithms to enhance lump dependent signals. Using published data, we fabricated simulated tissues with hard lesions of different diameters and embedding depths (Section IIIB, below), in order to mimic the presence of hard tumors in healthy tissue. We captured data from these samples using the sensing system, and evaluated the tactile imaging performance in three experiments. In the remainder of this section, we describe the tactile sensing system, the simulated tissues, the experiments and results.

A. Tactile Sensing System

We designed the sensing system to be comprised of four elements: the soft capacitive sensing array, a novel, custom suite of scanning and measurement electronics for data acquisition, a microcontroller for transferring data to the computer via serial communication, and a computer performing data processing, logging, and visualization of the data in real-time (Figure 5(a)). The resulting system (Fig. 5(b)) utilized custom electronics, and a commodity computing system in order to control the sensing.

The sensor was designed using the methods described above, and fabricated using soft lithography methods recently developed in our laboratory [23], yielding, in one embodiment, a 9×9 soft sensing array; other prototypes were similar but differed in the surface area and number of channels

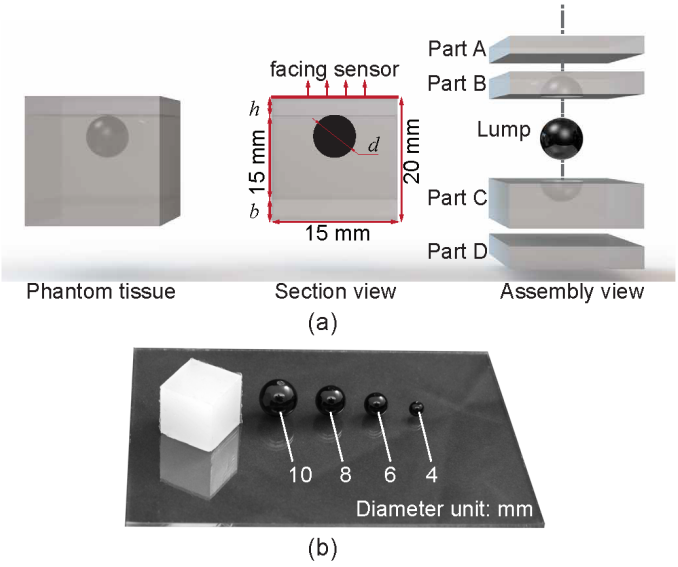

Fig. 6: Simulated tissues (a,b) with stiff solid ball of diameter d embedded with the 15 mm $\times$ 15 mm $\times$ 20 mm soft polymer cube, mimicking a lump in normal tissue. An extra layer of the same polymer material on top of the cube ensures the solid ball was embedded at depth h. Overall size was held constant.

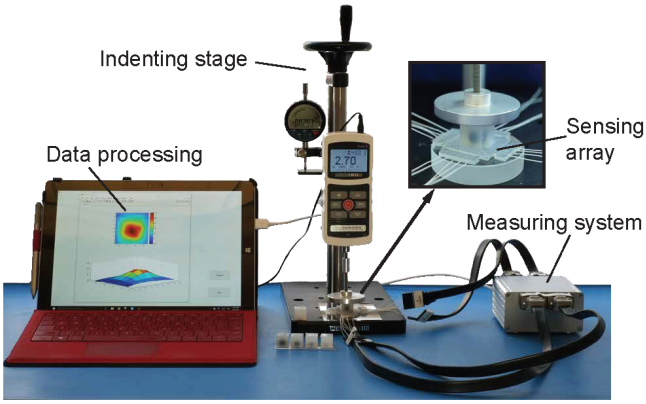

Fig. 7: Overview of the experiment setup, consisting of three functional parts: measuring system, indenting stage, and a PC for data processing. The measuring system includes a sensor array and the customized electronics.

(Fig. **??**). Upper and lower layers of microchannels in the sensor (microchannel diameter 300 μm, inter-channel spacing 2 mm) are embedded in polymer layers of 500 μm thickness; see Figure 4 (c-f). The micropillar layer, which provides enhanced sensitivity, linearity and operating range to the device, had a thickness of 600 μm, and contained an array of 8×8 micropillar structures (width 1 mm).

The data acquisition system used custom electronics with an integrated circuit for capacitance measurement (AD7746, Analog Devices) based on delta-sigma modulation analog-to-digital conversion, and yielding about 21 bits of effective resolution. The capacitance sensing limit was as small as tens of femtofarad (fF), with a resolution of 10^{-18} F. We designed a four-layer printed circuit board (Figure 5(c)) for the acquisition system, which is capable of reading up to 256 (16×16) sensing elements using high-speed 1:16 multiplexers with low series resistances to address each sensing element, and selecting respective pairs of orthogonal channels for measurement.

Due to the very small capacitances, accurate measurement required careful control over the parasitic parameters of the signal path between the sensing array and the measurement circuit. To this end, we designed custom electronics, custom shielded cabling and interconnects, and separate shielding (Figure 5(c)) for the measuring PCB and microcontroller, which carry analog signals and digital signals, respectively. The shielding ensures that parasitic capacitances at the cables play a small role compared to the dielectric environment near the sensor.

To address the latter, we also implemented an active switched-grounding isolation method controlled by the measurement circuit that suppressed interference in the measurements. While one sensing element (two microchannels) are being measured, idle channels are grounded, reducing fringing capacitance and crosstalk. The dynamic range of the assembled sensing system was empirically determined to be high, with a signal-to-noise ratio of 60 dB.

Data transfer from the sensing circuit to the computer was performed via serial communication from an embedded computing platform (Arduino Due, Arduino), which facilitated scanning through the sensing elements, and updating capacitance measurement with an effective sample rate of approximately 80 Hz. Custom software on a personal computer communicated with the microcontroller board, receiving, logging, visualizing, and analyzing the data.

B. Simulated Tissue Samples

To evaluate lump imaging with the developed soft tactile sensing system, we prepared a set of simulated tissue samples. These were modeled on mechanical and geometric properties of experimentally measured prostate tissue and tumors [8, 42] and were similar to phantom tissues used in prior studies on mechanical imaging of lumps [14, 43, 44]. We fabricated simulated tissues with soft polymer (Ecoflex 00-30, Smooth-on, Inc.; M100 modulus of 7×10^4 Pa). Samples included stiff lumps, in the form of solid balls (Young's modulus 5×10^{10} Pa) of varying radius for the experiments on lump imaging (Figure 6). This material is stiffer than a biological tumor, but it provides an appropriate contrast in stiffness to the soft polymer, and facilitates comparison with results from prior literature. Simulated tissues were fabricated with dimensions of 15 mm (width) $\times$ 15 mm (length) $\times$ 20 mm (height). We fabricated an array of tissues that varied in the depth h from the sample surface to the top of the lump and the diameter d of the solid ball. The lump was first embedded in a tissue of 15 mm high in a single step cast. Then, cover layers of thickness h and b, made of the same polymer material, were combined with the lump tissues on the top and bottom surfaces. The sum of the thickness of the two cover layers was 5 mm (i.e., $h + b = 5$ mm), ensuring that the resulting tissue height was height 20 mm.

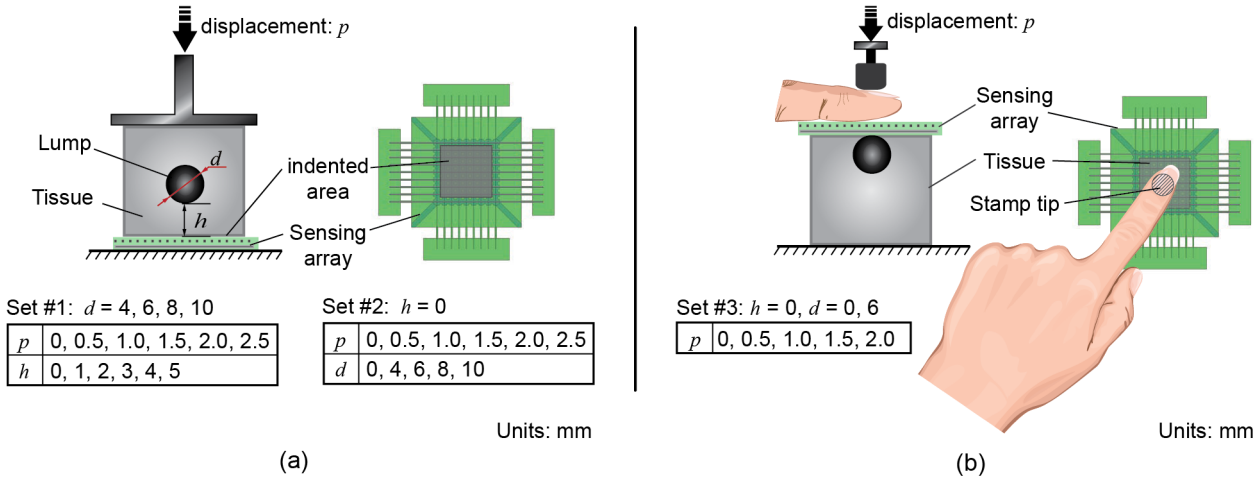

Fig. 8: A summary of the conditions used in the experiments. (a) Imaging lumps in simulated tissue, while varying diameter d, embedding depth h, and indenting displacement p. Experiment 1 varied p and h while fixing d. A blank sample ($d = 0$ mm) and four lump containing samples ($d = 4, 6, 8, 10$ mm) were used. Experiment 2 varied lump diameter at $h = 0$. (b) Imaging was performed as the sensor was loaded via a finger ($h = 0$ mm, $d = 0, 6$ mm).

In previous prostate cancer research, among 184 radical prostatectomy specimens, the maximum tumor diameter ranged from 0.1 to 4.1 cm (median, 1.6 cm) [44]. In this research, we selected four values of d in the experiment: $d =$ 4, 6, 8, 10 mm, which are on the small side of the range of observed prostate tumor sizes. Five values of embedding depth h (the distance between the tissue surface and the top of the ball) were used: $h =$ 0, 1, 2, 3, 4, 5 mm. In total, we fabricated 24 distinct simulated tissue samples including lumps, and one blank tissue with no lump, all of which were used in our experiments.

C. Tactile Image Capture and Enhancement

In lump imaging experiments, we applied the soft tactile sensor to simulated tissue samples, under mechanical or human control, using a range of displacements. We obtained data, in the form of tactile images, from the sensor, and processed this data to enhance lump contrast in the images.

The sensor and samples were aligned on a level platform. We used a high resolution force test stand (ES-20 and M5-20, Mark-10, Inc.) to apply vertical indentation displacement to the tissue. At each displacement value, the sensor data were captured, logged, and employed in a visualization system using a custom software graphical user interface (Figure 7).

We designed three sets of lump imaging experiments to evaluate the performance of the tactile sensing system. The first two imaged samples with lumps that varied in depth h (measured from the top of the lump to the surface of the tissue) and diameter d. In these experiments, we applied strain-controlled loading via an aluminum indenting plate (Figure 8a). In the third set of experiments, loading was provided by a human finger (Figure 8b), in order to provide a preliminary assessment of the utility of wearable sensing for tactile imaging.

The first set of experiments employed tissues with a fixed lump size (diameter $d =$ 10 mm) at different depths ($h =$ 1, 2, 3, 4, 5 mm). Tissues were was indented under strain-controlled loading from 0 mm to 2.5 mm while sensor data was logged. In a second set of experiments, the embedding depth was held constant (depth $h = 0$ mm, corresponding to lumps just below the surface), and lump diameter was varied ($d =$ 0, 4, 6, 8, 10 mm). In the last set of experiments, loading of the sensor was provided by a human finger, while the level of displacement was controlled by (comfortably) affixing it to the precision indenting rig (Figure 8(b)). Five displacement values were used in testing (0, 0.5, 1.0, 1.5, 2.0 mm).

The captured data had spatial resolution of 2 mm (total 81 spatial samples, 9×9 array), and we smoothed the captured data via a moving average over ten frames of sensing data. To increase the contrast of the imaged lumps and render them more robust to differences in lump depth or loading we computed enhanced images, by interpolating the raw measurements, performing normalization, and background subtraction. First, we formed high resolution images via linear interpolation, yielding values $f(x, y)$ of the image at interpolated points (x, y) from those at measurement points (x_i, y_i), $i = 1, 2$, which are position coordinates of the sensing elements, and $f(x_i, y_i)$, $i = 1, 2$, the measured values of capacitance change.

Subsequently, using this data, we implemented a background subtraction method that removed the signal produced by loading of the bulk tissue from that due to the lumps. The same method may prove useful for mitigate effects of support geometry and mechanics. For the background signal, we employed recorded blank (no-lump) tactile images $\hat{f}(x, y; z)$ for each load value z. These images were subtracted from the measured signals $f(x, y; z)$ at the same load value, yielding enhanced images $I(x, y; z)$

$$I(x, y; z) = \frac{f(x, y; z)}{\max_{x,y} f(x, y; z)} - \frac{\hat{f}(x, y; z)}{\max_{x,y} \hat{f}(x, y; z)} \quad (1)$$

It is often desirable to obtain a quantitative estimate of lump size from image data. Since even those images produced by

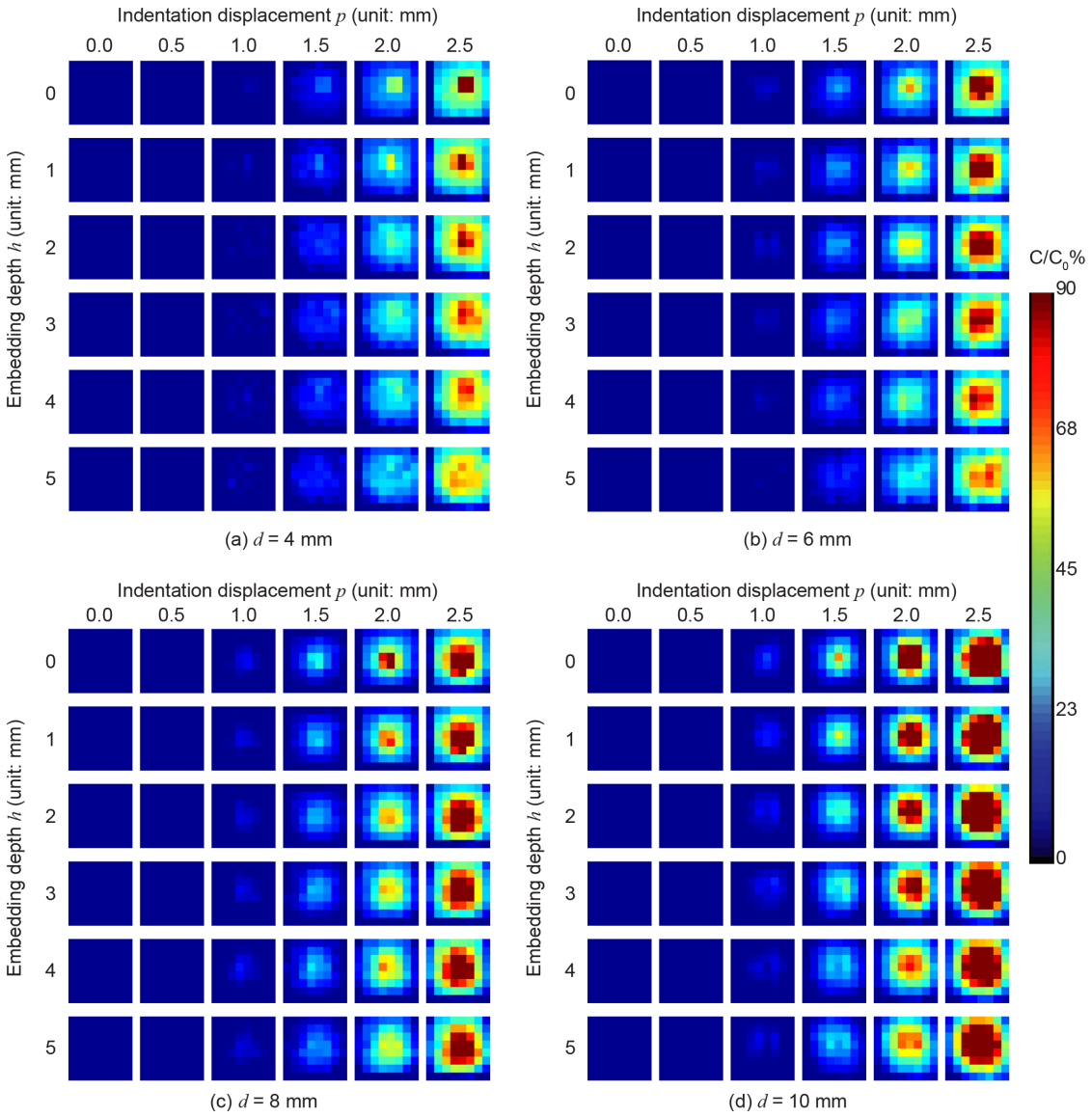

Fig. 9: Tactile images (a-d) captured for tissues of four lump diameter values ($d = 4, 6, 8, 10$ mm) as indenting displacement and depth were varied. Depth was measured from the top of the lump to the surface of the tissue ($h = 0, 1, 2, 3, 4, 5$ mm). Indenting displacement p is shown over a range from 0 mm to 2.5 mm in steps of 0.5 mm. For each lump size, the highlighted signal in the capacitance change map that reflects the subsurface lump becomes more prominent as the depth h decreases or the indentation increases. At equal values of depth and displacement, a larger lump size yields a higher capacitance value, and wider extent of the area in which this increase is observed.

spherical lumps are not perfectly circular, we associate an equivalent lump diameter d_e to the image of a lump, which we define to be the diameter of a disk of diameter d_e whose area A is equal to the area of the region of the image covered by the lump, which is given by

$$A = \pi d_e^2/4 \quad \Rightarrow \quad d_e = \sqrt{4A/\pi} \tag{2}$$

The area A is not known. To estimate it, we used a method from prior literature [14], in which the lump image is modeled via a two-dimensional Gaussian function, whose parameters are fit to the data. The fit function is given by

$$f(x, y) = f_0 + a \exp\left(-\frac{(x - x_c)^2}{2w_1^2} - \frac{(y - y_c)^2}{2w_2^2}\right) \tag{3}$$

An example is shown in Figure 10. We fit the differential image with the Gaussian function, which is then evaluated on a dense mesh (spacing 0.2 $\times$ 0.2 mm), and we estimated the image area A corresponding to the lump via the proportion of pixels that lie above the threshold. The value d_e is computed using equation 2.

In a last set of experiments, in order to demonstrate the feasibility of wearable tactile sensing, sensing was performed via a human finger, which applied the soft tactile sensor to the sample under strain-controlled loading in the normal direction (Figure 8b). Image data was collected from samples with lumps of diameter $d = 10$ mm, embedding depth $h = 0$ mm, and indentation displacements from 0.5 to 2.0 mm.

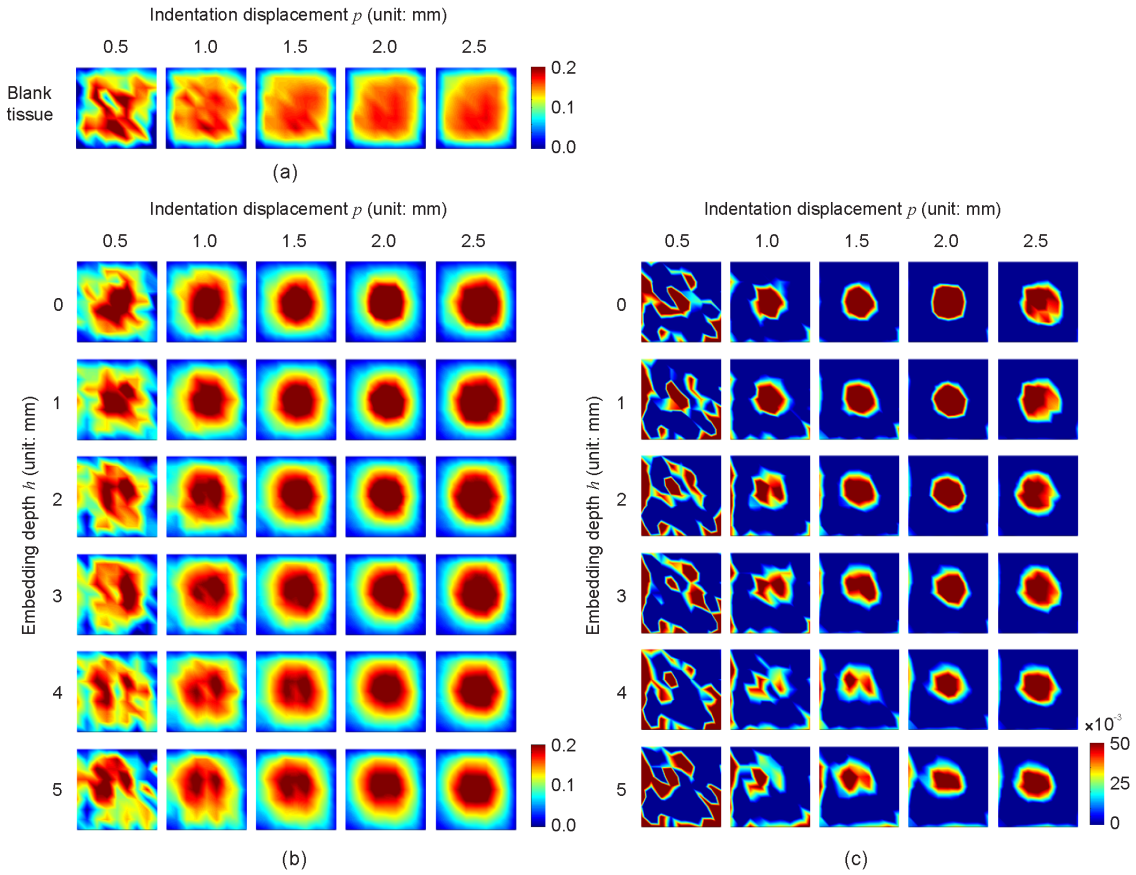

Fig. 11: Enhancement of the tactile pattern in the data of tissue samples embedded with lump ($d = 10$ mm). a, b) Normalized tactile image data. c) Enhanced image, obtained by subtracting the normalized blank tissue image from the lump image.

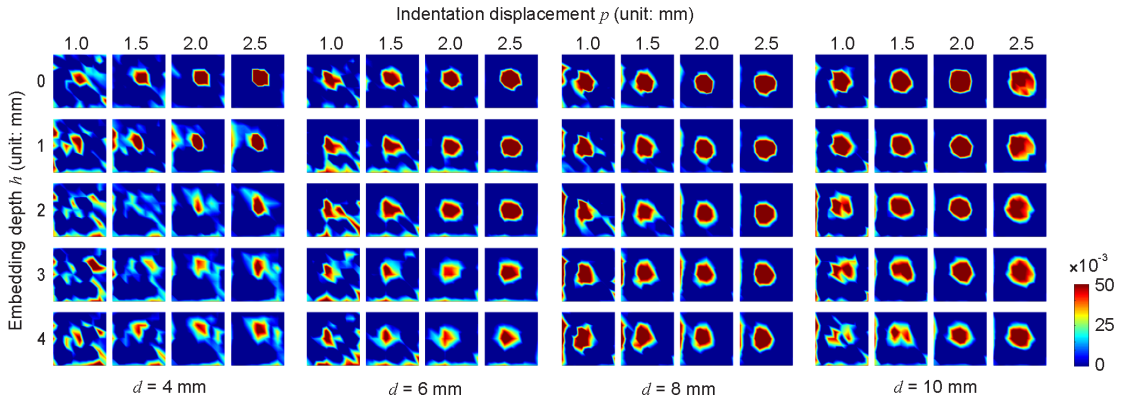

Fig. 12: Enhancement of the tactile pattern in the data of tissue samples embedded with lumps of four different diameters ($d = 4, 6, 8, 10$ mm).

IV. Results and Discussion

The experiments imaged simulated tumor-containing tissue with lumps of varying diameters. We compared the results with and without lumps, the latter consisting of blank tissue samples (Fig. **??**b). When present, the lump was a prominent central feature in tactile images of all of the samples that possessed it. For these lump-containing tissues (Fig. 9), the tactile images clearly manifest the presence of the lump upon indentation of at least 1.5 mm. For larger or shallower lumps, their presence was revealed with even lower levels of indentation. In contrast, the blank tissues (Fig. **??**b) showed little spatial differentiation up to an indentation of 1.5 mm; beyond this, there was a broad increase in signal in the central area, where strain was larger, but those spatial changes were slowly varying. We note that the color mapping in this figure extends to a maximum value of $C/C_0 = 110\%$, but that this does not represent saturation in the sensor output. Instead, capacitance grows monotonically at high loads as predicted by theory [23].

For lump-containing tissues, as the lumps varied in depth, there was an increase in capacitance in the lump region of

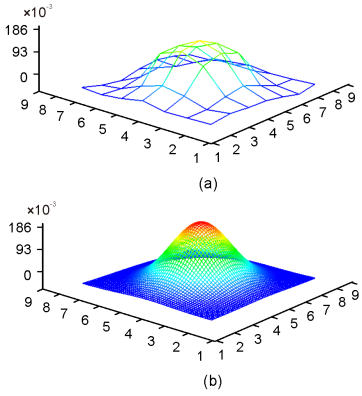

Fig. 10: Image production from a lump is modeled via fitting a 2D Gaussian function (a), which was then evaluated on a fine mesh (b) in order to estimate the projected area of the lump.

the image, and the increase grew with decreased embedding depth, yielding a qualitatively clearer image for lumps that were closer to the surface (Figure 9).

The contrast-enhanced images were computed using equation 1 by subtracting normalized reference (blank sample) tactile images from normalized measured images (Figure 11). The results provide high contrast and definition of the lump region, capturing the lump shape and size even when the lump was small or deeply embedded (Figure 12).

We used the enhanced images (Fig. 12) to compute effective lump diameters d_e at each embedding depth, lump size, and indentation level using the Gaussian fitting method of equation (3) and diameter estimate of equation 2. We combined data from all conditions, and computed a histogram of estimated values relative to the true diameter values d_e/d (Fig. 13). The results indicate that the estimates predict the true lump size with an accuracy of a few percent, irrespective of the embedding depth, lump size, or indentation. The standard deviation across all conditions was 12%, indicating that this size estimate was robust to the lump parameters and palpation method (Fig. 13).

In a last set of experiments, we provide preliminary data investigating the utility of the soft sensing system described here for wearable sensing during physical examination by palpation. The resulting images reflect the geometry and properties of the finger, but also clearly evidence the presence of the lump, when the latter is embedded in the simulated tissue (Figure 14) and when the indenting depth is sufficiently high (more than about 1.5 mm). As noted in Section II, the geometry and mechanics of the surface that supports the sensor affects the sensor performance, since sensor output increases with internal strain. In manual tissue palpation, movement behavior also plays a significant role in determining the tactile information that is acquired [45], although we have not examined these factors here.

V. Conclusion

This study investigated the utility of soft tactile sensors for imaging lumps in simulated tissue. We presented new methods for tactile imaging, including a integrated electronic sensing system that achieves high levels of sensitivity. Lumps manifested clearly in tactile imaging, even under gentle palpation, which is important in applications involving delicate or sensitive tissues.

Using data from this system, and algorithms for extracting invariant signatures of subsurface lumps, we demonstrated that it is possible to robustly image such lumps. This could be done in a manner that is largely independent of the depth at which they are embedded, or the applied load. We also showed that the resulting images can be used to estimate the size of the lump accurately, with a population mean within 2% under the controlled conditions of our study, and standard deviation of just 12%, even for small, deeply embedded lumps.

We also provided preliminary data motivating the feasibility of tactile imaging with a wearable sensor. Such a sensor could one day prove useful in clinical examinations by palpation, where they could provide quantitative documentation that is otherwise lacking in most examinations. One instructive case example is digital rectal examination of the prostate, a common physical examination for men, which often provides one of the earliest means of detecting cancer. The sensing system presented here can be designed and fabricated with the flexibility to accommodate applications requiring different ranges of movement and applications.

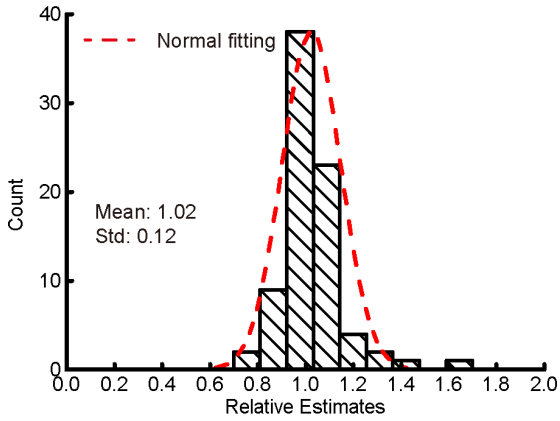

Fig. 13: Estimated lump diameter relative to true diameter, d_{est}/d, for all samples (4, 6, 8, 10 mm), using the method of equations (2)-(3). The distribution is narrowly peaked about the true value (2% error), and a standard deviation of 12%, evidencing the effectiveness of the tactile image enhancement algorithm at imaging lumps independent of embedding depth or palpation firmness.

The results of this research are promising, but there remain several limitations that may be improved upon in future work. While the processing presented here is quasi-static, the rate of change in the signals captured by the sensor (for example, the growth rate of contact area or strain energy density) is known to be salient to human stiffness perception. Such data could readily be captured dynamically in order to provide further information about the mechanical properties of palpated tissues. In human palpation, shear stress also plays an important sensory role, and could prove useful for me-

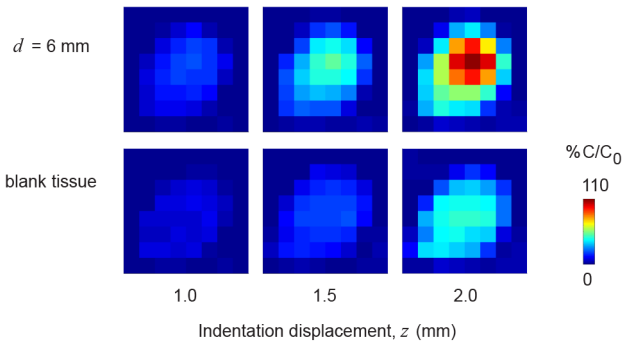

Fig. 14: Tactile images of simulated tissue captured under loading by a human finger (Fig. 8b), at three indentation levels, with and without embedded lump (diameter 6 mm, depth 0 mm).

chanical imaging applications. The sensing method explored here proves adept at capturing stresses in the normal direction, and it may be useful to explore new features, comprising additional functional layers or structures, that could facilitate shear stress imaging. Tactile imaging can be effective at capturing lump geometry from surface measurements, but the three-dimensional, irregular nature of some tumors would pose significant challenges. Mechanically, if the sensor support is elastic, the geometry of the sensor can vary during palpation. Further investigation could be warranted to understand how this could affect sensor performance.

The electronic system presented here achieved high signal-to-noise ratio, high sensitivity, and real-time capture, but in a commercial application, even faster performance could be desirable, as might readily be achieved within the state of the art, using more customized data acquisition integrated circuitry. New materials for electric shielding, such as elastic conductive polymer layers, would further aid in insulating the sensor from fringing capacitance effects. Finally, in order to facilitate the translation of this work to applications in healthcare, experiments involving excised or in-vivo tissue samples would be especially valuable in order to establish a foundation for the clinical application of mechanical imaging with compliant tactile sensors.

ACKNOWLEDGMENTS

This work was supported by NSF awards No. 1623459 and 1628831.

REFERENCES

[1] I. Barman and S. K. Guha, "Analysis of a new combined stretch and pressure sensor for internal nodule palpation," *Sensors and Actuators A: Physical*, vol. 125, no. 2, pp. 210–216, 2006.

[2] T. A. Krouskop, T. M. Wheeler, F. Kallel, B. S. Garra, and T. Hall, "Elastic moduli of breast and prostate tissues under compression," *Ultrasonic Imaging*, vol. 20, no. 4, pp. 260–274, 1998.

[3] S. Phipps, T. Yang, F. Habib, R. Reuben, and S. McNeill, "Measurement of tissue mechanical characteristics to distinguish between benign and malignant prostatic disease," *Urology*, vol. 66, no. 2, pp. 447 – 450, 2005.

[4] K. Hoyt, B. Castaneda, M. Zhang, P. Nigwekar, P. A. di Santa Agnese, J. V. Joseph, J. Strang, D. J. Rubens, and K. J. Parker, "Tissue elasticity properties as biomarkers for prostate cancer," *Cancer biomarkers: Section A of Disease markers*, vol. 4, no. 4-5, pp. 213–225, 2008.

[5] A. L. Trejos, J. Jayender, M. T. Perri, M. D. Naish, R. V. Patel, and R. A. Malthaner, "Experimental evaluation of robot-assisted tactile sensing for minimally invasive surgery," in *Biomedical Robotics and Biomechatronics, 2008. BioRob 2008. 2nd IEEE RAS & EMBS International Conference on*, Conference Proceedings, pp. 971–976.

[6] P. Puangmali, K. Althoefer, L. D. Seneviratne, D. Murphy, and P. Dasgupta, "State-of-the-art in force and tactile sensing for minimally invasive surgery," *IEEE Sensors Journal*, vol. 8, no. 4, pp. 371–381, 2008.

[7] A. L. Trejos, J. Jayender, M. T. Perri, M. D. Naish, R. V. Patel, and R. A. Malthaner, "Robot-assisted tactile sensing for minimally invasive tumor localization," *The International Journal of Robotics Research*, vol. 28, no. 9, pp. 1118–1133, 2009.

[8] A. P. Astrand, V. Jalkanen, B. M. Andersson, and O. A. Lindahl, "Detection of stiff nodules embedded in soft tissue phantoms, mimicking cancer tumours, using a tactile resonance sensor," *Journal of Biomedical Science and Engineering*, vol. 7, no. 4, pp. 181–193, 2014.

[9] M. S. Arian, C. A. Blaine, G. E. Loeb, and J. A. Fishel, "Using the biotac as a tumor localization tool," in *Proc. IEEE Haptics Symposium*, 2014, pp. 443–448.

[10] J. C. T. Hui and K. J. Kuchenbecker, *Evaluating the BioTacs Ability to Detect and Characterize Lumps in Simulated Tissue*. Berlin, Heidelberg: Springer Berlin Heidelberg, 2014, pp. 295–302.

[11] H. Liu, D. P. Noonan, B. J. Challacombe, P. Dasgupta, L. D. Seneviratne, and K. Althoefer, "Rolling mechanical imaging for tissue abnormality localization during minimally invasive surgery," *IEEE Transactions on Biomedical Engineering*, vol. 57, no. 2, pp. 404–414, 2010.

[12] J.-H. Lee and C.-H. Won, "High-resolution tactile imaging sensor using total internal reflection and nonrigid pattern matching algorithm," *Sensors Journal, IEEE*, vol. 11, no. 9, pp. 2084–2093, 2011.

[13] X. Jia, R. Li, M. A. Srinivasan, and E. H. Adelson, "Lump detection with a gelsight sensor," in *Proc. World Haptics Conference*, 2013, pp. 175–179.

[14] J. C. Gwilliam, Z. Pezzementi, E. Jantho, A. M. Okamura, and S. Hsiao, "Human vs. robotic tactile sensing: Detecting lumps in soft tissue," in *Proc. IEEE Haptics Symposium, 2010*, pp. 21–28.

[15] M. Beccani, C. Di Natali, L. J. Sliker, J. A. Schoen, M. E. Rentschler, and P. Valdastri, "Wireless tissue palpation for intraoperative detection of lumps in the soft tissue," *IEEE Transactions on Biomedical Engineering*, vol. 61, no. 2, pp. 353–361, 2014.

[16] V. Egorov and A. P. Sarvazyan, "Mechanical imaging of the breast," *IEEE Transactions on Medical Imaging*, vol. 27, no. 9, pp. 1275–1287, 2008.

[17] Y.-L. Park, C. Majidi, R. Kramer, P. Brard, and R. J. Wood, "Hyperelastic pressure sensing with a liquid-embedded elastomer," *Journal of Micromechanics and Microengineering*, vol. 20, no. 12, p. 125029, 2010.

[18] P. Yong-Lae, C. Bor-Rong, and R. J. Wood, "Design and fabrication of soft artificial skin using embedded microchannels and liquid conductors," *IEEE Sensors Journal*, vol. 12, no. 8, pp. 2711–2718, 2012.

[19] P. J. Codd, A. Veaceslav, A. H. Gosline, and P. E. Dupont, "Novel pressure-sensing skin for detecting impending tissue damage during neuroendoscopy," *J Neurosurg Pediatr*, vol. 13, no. 1, pp. 114–21, 2014.

[20] J. B. Chossat, P. Yong-Lae, R. J. Wood, and V. Duchaine, "A soft strain sensor based on ionic and metal liquids," *IEEE Sensors Journal*, vol. 13, no. 9, pp. 3405–3414, 2013.

[21] A. Fassler and C. Majidi, "Soft-matter capacitors and inductors for hyperelastic strain sensing and stretchable electronics," *Smart Materials and Structures*, vol. 22, no. 5, p. 055023, 2013.

[22] B. Li, A. K. Fontecchio, and Y. Visell, "Mutual capacitance of liquid conductors in deformable tactile sensing arrays," *Applied Physics Letters*, vol. 108, no. 1, p. 013502, 2016.

[23] B. Li, Y. Gao, A. Fontecchio, and Y. Visell, "Soft capacitive tactile sensing arrays fabricated via direct filament casting," *Smart Materials and Structures*, vol. 25, no. 7, p. 075009, 2016.

[24] R. D. Ponce Wong, J. D. Posner, and V. J. Santos, "Flexible microfluidic normal force sensor skin for tactile feedback," *Sensors and Actuators A: Physical*, vol. 179, pp. 62–69, 2012.

[25] D. J. Cohen, D. Mitra, K. Peterson, and M. M. Maharbiz, "A highly elastic, capacitive strain gauge based on percolating nanotube networks," *Nano Lett*, vol. 12, no. 4, pp. 1821–5, 2012.

[26] D. J. Lipomi, M. Vosgueritchian, B. C. Tee, S. L. Hellstrom, J. A. Lee, C. H. Fox, and Z. Bao, "Skin-like pressure and strain sensors based on transparent elastic films of carbon nanotubes," *Nat Nanotechnol*, vol. 6, no. 12, pp. 788–92, 2011.

[27] W. Hu, X. Niu, R. Zhao, and Q. Pei, "Elastomeric transparent capacitive sensors based on an interpenetrating composite of silver nanowires and polyurethane," *Applied Physics Letters*, vol. 102, no. 8, p. 083303, 2013.
[28] Y. Yao, S.; Zhu, "Wearable multifunctional sensors using printed stretchable conductors made of silver nanowires," *Nanoscale*, vol. 6, no. 4, p. 2345, 2014.
[29] O. A. Araromi, S. Rosset, and H. R. Shea, "High-resolution, large-area fabrication of compliant electrodes via laser ablation for robust, stretchable dielectric elastomer actuators and sensors," *ACS Applied Materials & Interfaces*, vol. 7, no. 32, pp. 18 046–18 053, 2015.
[30] D.-H. Kim, N. Lu, R. Ma, Y.-S. Kim, R.-H. Kim, S. Wang, J. Wu, S. M. Won, H. Tao, A. Islam, K. J. Yu, T.-i. Kim, R. Chowdhury, M. Ying, L. Xu, M. Li, H.-J. Chung, H. Keum, M. McCormick, P. Liu, Y.-W. Zhang, F. G. Omenetto, Y. Huang, T. Coleman, and J. A. Rogers, "Epidermal electronics," *Science*, vol. 333, no. 6044, pp. 838–843, 2011.
[31] N. L. J. A. R. Dae-Hyeong Kim, "Materials for multifunctional balloon catheters with capabilities in cardiac electrophysiological mapping and ablation therapy," *Nature Mater.*, vol. 10, no. 4, p. 316, 2011.
[32] J. W. Jeong, M. K. Kim, H. Cheng, W. H. Yeo, X. Huang, Y. Liu, Y. Zhang, Y. Huang, and J. A. Rogers, "Capacitive epidermal electronics for electrically safe, long-term electrophysiological measurements," *Adv Healthc Mater*, vol. 3, no. 5, pp. 642–8, 2014.
[33] Y. Ming, P. B. Andrew, L. Nanshu, S. Yewang, L. Rui, C. Huanyu, A. Abid, H. Yonggang, and A. R. John, "Silicon nanomembranes for fingertip electronics," *Nanotechnology*, vol. 23, no. 34, p. 344004, 2012.
[34] B. Li, Y. Shi, A. Fontecchio, and Y. Visell, "Assemblies of microfluidic channels and micropillars facilitate sensitive and stretchable tactile sensing," *IEEE Sensors Journal, In Press*.
[35] P. S. Wellman, E. P. Dalton, D. Krag, K. A. Kern, and R. D. Howe, "Tactile imaging of breast masses: first clinical report," *Archives of Surgery*, vol. 136, no. 2, p. 204, 2001.
[36] V. Egorov, H. van Raalte, and V. Lucente, "Quantifying vaginal tissue elasticity under normal and prolapse conditions by tactile imaging," *International urogynecology journal*, vol. 23, no. 4, pp. 459–466, 2012.
[37] J.-H. Lee and C.-H. Won, "High-resolution tactile imaging sensor using total internal reflection and nonrigid pattern matching algorithm," *IEEE Sensors Journal*, vol. 11, no. 9, pp. 2084–2093, 2011.
[38] A. Sarvazyan and V. Egorov, "Mechanical imaging-a technology for 3-d visualization and characterization of soft tissue abnormalities: A review," *Current medical imaging reviews*, vol. 8, no. 1, pp. 64–73, 2012.
[39] T. Yamamoto, B. Vagvolgyi, K. Balaji, L. L. Whitcomb, and A. M. Okamura, "Tissue property estimation and graphical display for teleoperated robot-assisted surgery," in *Robotics and Automation, 2009. ICRA'09. IEEE International Conference on*. IEEE, 2009, pp. 4239–4245.
[40] S. J. French, D. J. Saunders, and G. W. Ingle, "The system gallium-indium," *The Journal of Physical Chemistry*, vol. 42, no. 2, pp. 265–274, 1937.
[41] M. D. Dickey, R. C. Chiechi, R. J. Larsen, E. A. Weiss, D. A. Weitz, and G. M. Whitesides, "Eutectic gallium-indium (egain): A liquid metal alloy for the formation of stable structures in microchannels at room temperature," *Advanced Functional Materials*, vol. 18, no. 7, pp. 1097–1104, 2008.
[42] V. Jalkanen, B. Andersson, A. Bergh, B. Ljungberg, and O. Lindahl, "Prostate tissue stiffness as measured with a resonance sensor system: A study on silicone and human prostate tissue in vitro," *Medical & Biological Engineering & Computing*, vol. 44, no. 7, p. 593, 2006.
[43] R. T. Vollmer, "Tumor length in prostate cancer," *Am J Clin Pathol*, vol. 130, no. 1, pp. 77–82, 2008.
[44] M. D. L. Cheng, M. D. J. N. Eble, M. D. T. M. Ulbright, M. S. J. K. Daggy, M. D. M. O. Koch, and M. D. L. E. Eichelberger, "Predicting tumor volume in radical prostatectomy specimens from patients with prostate cancer," *American Journal of Clinical Pathology*, vol. 120, no. 3, pp. 386–391, 2003.
[45] J. Konstantinova, M. Li, G. Mehra, P. Dasgupta, K. Althoefer, and T. Nanayakkara, "Behavioral characteristics of manual palpation to localize hard nodules in soft tissues," *IEEE Transactions on Biomedical Engineering*, vol. 61, no. 6, pp. 1651–1659, 2014.

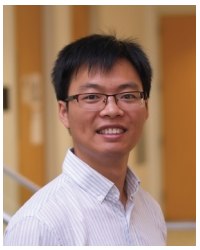

Bin Li received his B.S. and M.S. degrees in electronic science and technologies, and physical electronics from Xi'an JiaoTong University, Xi'an, China, in 2006 and 2009 respectively. He was electronics engineer from 2009 to 2012 in the Optical Network R&D department at Huawei Technologies in Shenzhen, China. Since 2012, he has worked in the Nanophotonics Laboratory and RE Touch Laboratory at Drexel University, where he is a Ph.D. candidate in Electrical and Computer Engineering. His research interests include the design and fabrication of novel wearable electronics and tactile sensing systems integration, with applications in haptics, clinical palpation, prosthetics, and humanoid robotics.

Ye Shi Ye Shi received the B.Sc. degree in Automation from Harbin Institute of Technology, China in 2013, and M.S. degree in Electrical Engineering from Drexel University, Philadelphia, PA, USA, in 2016. He has been a student researcher at the RE Touch Lab and the Drexel Nanophotonics Lab since 2015. His interests include control, systems, machine learning, robotics and haptics. His current research includes system optimization, image processing, electronics design, data analysis and soft electronics.

Adam Fontecchio Dr. Adam Fontecchio is a Professor in the Electrical and Computer Engineering Department at Drexel University and is Vice-Dean of the Graduate College. He is the inaugural Director of the Center for the Advancement of STEM Teaching and Learning Excellence (CASTLE), currently serves as Vice-Chair of the IEEE Philadelphia Section, and is a member of the IEEE-USA K-12 STEM Literacy Committee. His research focuses on the area of nanophotonics. He has served as PI or Co-PI on $>$ \$18M in sponsored research funding, and authored $>$90 peer-reviewed papers. He was selected as the 2015 Delaware Valley Engineer of the Year, and is also the recipient of a NASA New Investigator Award, the Drexel Graduate Student Association Outstanding Mentor Award, the Drexel University ECE Outstanding Research Achievement Award and the International Liquid Crystal Society Multimedia Prize.

Yon Visell received the PhD Degree in Electrical and Computer Engineering from McGill University (2011), and MA and BA degrees in Physics (Univ. Texas-Austin, Wesleyan Univ.). Since 2015, he is Assistant Professor of Media Arts and Technology, Electrical and Computer Engineering, and Mechanical Engineering (by courtesy) at the University of California, Santa Barbara, where he directs the RE Touch Lab. Assistant Professor (2012-2015) in the ECE Department at Drexel University. Post-Doctoral Fellow (2011-2012) at the Inst. of Intelligent Systems and Robotics, Université Pierre et Marie Curie. He has been employed in industrial R&D for sonar, speech recognition, and music DSP at several high-technology companies. His research interests include whole-hand haptic function, haptic engineering, and soft robotics.